

Molecular nanomechanics of nascent bone: fibrillar toughening by mineralization

Markus J Buehler

Laboratory for Atomistic and Molecular Mechanics, Department of Civil and Environmental Engineering, Massachusetts Institute of Technology, 77 Massachusetts Avenue, Room 1-272, Cambridge, MA 02139, USA

E-mail: mbuehler@MIT.EDU

Received 16 April 2007, in final form 24 May 2007

Published 20 June 2007

Online at stacks.iop.org/Nano/18/295102

Abstract

Mineralized collagen fibrils are highly conserved nanostructural building blocks of bone. By a combination of molecular dynamics simulation and theoretical analysis it is shown that the characteristic nanostructure of mineralized collagen fibrils is vital for its high strength and its ability to sustain large deformation, as is relevant to the physiological role of bone, creating a strong and tough material. An analysis of the molecular mechanisms of protein and mineral phases under large deformation of mineralized collagen fibrils reveals a fibrillar toughening mechanism that leads to a manifold increase of energy dissipation compared to fibrils without mineral phase. This fibrillar toughening mechanism increases the resistance to fracture by forming large local yield regions around crack-like defects, a mechanism that protects the integrity of the entire structure by allowing for localized failure. As a consequence, mineralized collagen fibrils are able to tolerate microcracks of the order of several hundred micrometres in size without causing any macroscopic failure of the tissue, which may be essential to enable bone remodelling. The analysis proves that adding nanoscopic small platelets to collagen fibrils increases their Young's modulus and yield strength as well as their fracture strength. We find that mineralized collagen fibrils have a Young's modulus of 6.23 GPa (versus 4.59 GPa for the collagen fibril), yield at a tensile strain of 6.7% (versus 5% for the collagen fibril) and feature a fracture stress of 0.6 GPa (versus 0.3 GPa for the collagen fibril).

(Some figures in this article are in colour only in the electronic version)

1. Introduction

Hierarchical structures in biological materials such as spider silk, muscle tissue or skin feature distinct architectural features that extend through all length scales, from nanoscale to macroscale. Proteins are the key molecular building blocks of such biological matter and they play a vital role in making these materials lightweight, yet strong, elastic and tough.

One of the most intriguing protein materials found in nature is bone, a material composed out of assemblies of tropocollagen molecules and tiny hydroxyapatite crystals, forming an extremely tough, yet lightweight material [1–3].

Bone has evolved to provide structural support to organisms, and therefore, its mechanical properties are of great physiological relevance.

Figure 1 depicts the geometry of the nanostructure of bone, showing several hierarchical features from atomic scale to microscale. The smallest scale hierarchical features of bone include the protein phase composed of tropocollagen (TC) molecules and collagen fibrils (CFs) as well as mineralized collagen fibrils (MCFs) (see figure 1). Tropocollagen molecules assemble into collagen fibrils in a hydrated environment, which mineralize by formation of hydroxyapatite (HA) crystals in the gap regions that exist due to the staggered

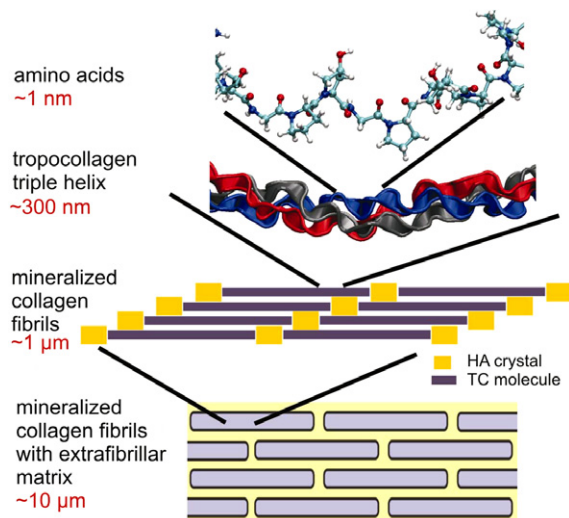


Figure 1. Geometry of the nanostructure of bone, showing several hierarchical features from atomic scale to microscale. A simple schematic diagram is given of the hierarchical structure of mineralized collagen fibrils, forming the most basic building block of bone [1, 3]. Three polypeptide strands arrange to form a triple helical tropocollagen molecule. Tropocollagen molecules assemble into collagen fibrils in a hydrated environment, which mineralize by formation of hydroxyapatite (HA) crystals in the gap regions that exist due to the staggered geometry. Mineralized collagen fibrils combine with the extrafibrillar matrix to fibril arrays, which form fibril array patterns [1, 3, 8]. Typically, a total of seven hierarchical levels are found in bone. The present work is limited to the scale of mineralized fibrils, with the objective of providing insight into the most fundamental scales of bone and its deformation mechanics under tensile loading.

geometry. MCFs arrange together with an extrafibrillar matrix (EFM) to form the next hierarchical layer of bone. While the structures at scales larger than MCFs vary for different bone types, mineralized collagen fibrils are highly conserved, nanostructural primary building blocks of bone that are found universally [3–7]. Each MCF consists of TC molecules with approximately 300 nm length, arranged in a characteristic staggered pattern. Gap regions in this arrangement are filled with tiny hydroxyapatite (HA) crystals. The present work is limited to the scale of mineralized fibrils, with the objective of providing insight into the most fundamental scale of bone and its deformation mechanics under tensile loading.

The mechanical properties of bone have received significant attention. Particular effort has been devoted to understanding the mechanisms that make bone tough. Whereas some experimental evidence suggests that the sub-micrometre structure is critical for the mechanical properties of macroscopic bone [5, 7–13], other results indicate that macroscopic mechanisms such as crack bridging or microcracking [14–17] contribute to the toughness of bone. Concepts such as sacrificial bonds and hidden length [10, 11, 18] suggest toughening mechanisms that occur between different mineralized collagen fibrils.

However, due to the structural complexity of bone, the analysis and quantification of the deformation mechanisms at the ultra-scale of individual mineralized collagen fibrils (MCFs) remains an area that is not well understood. Limited



Figure 2. Overview of the two structures considered here; subplot (a) shows a CF and subplot (b) shows an MCF. The structures are loading in uniaxial tension along the axis of the TC molecules.

knowledge exists about whether, and if yes, how, molecular-scale mechanisms within single MCFs contribute to the toughness and stiffness of bone, as well as for its ability to repair itself. The effect of precipitating mineral crystals during bone formation remains unknown.

Most theoretical and computational analyses of bone have been carried out at continuum scales [19], neglecting the particular complexities of molecular interactions and chemistry. To date, there exists no molecular model of the nanostructure of bone that enables a rigorous linking between molecular and tissue scales. It is emphasized that previous atomistic and molecular models of collagen fibrils have not included any mineral phase [20–22].

In the studies reported here, a simple molecular model of MCFs is utilized that provides a fundamental description of its nanomechanical properties. The small and large deformation mechanics of a pure collagen fibril and a mineralized collagen fibril are systematically compared (see figure 2). Both structures are subject to identical tensile loading in the direction of the molecular axis of the TC molecules. Comparing the deformation mechanisms, stress–strain behaviour and energy dissipation reveals insight into the effect of mineralization. It is found that mineralization leads to an increase in stiffness, yield stress, fracture stress and energy dissipation. The study reveals how a highly dissipative, yet strong material can be formed out of a soft polymeric collagen phase and hard, brittle HA by arranging molecules and crystals at characteristic nanostructured length scales.

2. Computational model

The computational model is developed with the aim of elucidating the generic behaviour and deformation mechanisms of MCFs.

2.1. Model geometry

The model is a simple two-dimensional (2D) system of a mineralized collagen fibril, based on an earlier model of pure collagen fibrils [21], extended to describe an additional mineral phase. The CF consists of a staggered array of TC molecules. The gap zones in the CF [3, 8, 23] are filled with a single crystal that has a planar size of approximately $28 \text{ nm} \times 1.4 \text{ nm}$, filling the entire open space, resembling the presence of the HA phase, leading to an MCF.

It is noted that, as bone is formed, mineral crystals exceed the size of the gap region and penetrate into the collagen phase. The present study does not include these effects, and is thus limited to the early stages of bone formation (‘nascent bone’).

The term ‘hydroxyapatite’ (HA) is used to refer to the mineral phase in bone, although this component is also referred to as ‘dahllite’ or carbonated apatite [3].

References [20, 21] describe a molecular model developed to describe the molecular mechanics of collagen fibrils, by explicitly considering the molecular architecture. This molecular model serves as the basis for the model developed and used for the studies reported in the present paper. However, the work reported in [20, 21] does not contain any studies of MCFs. This paper presents the first molecular-scale model of the nanostructure of bone. The experimental paper [23] considers a geometry that is closest to the one considered in the present paper. However, to the best of our knowledge no other molecular-scale model of the nanostructure of bone has been reported thus far.

2.2. Molecular model of mineralized collagen fibrils

The studies are carried out using a reactive mesoscopic model describing TC molecules as a collection of beads interacting according to interparticle multi-body potentials; the pure collagen model described in [21] is extended here to describe the HA phase and HA–TC interactions. The equations of motion are solved according to a classical molecular dynamics (MD) scheme [24] implemented in the LAMMPS simulation code [25].

The total potential energy of the model is

$$E = E_T + E_B + E_{TC} + E_{HA} + E_{HA-TC}. \quad (1)$$

The terms E_T and E_B are only applied within the TC molecules. The bending energy between the three beads of a TC molecule is

$$\phi_B(\varphi) = \frac{1}{2}k_B(\varphi - \varphi_0)^2, \quad (2)$$

with k_B relating to the bending stiffness of the molecule. The nonlinear stress–strain behaviour of individual TC molecules under tensile loading is approximated with a bilinear model (the energy E_T is given by integrating the force $F_T(r)$ over the radial distance) [20]. The force between two particles is

$$F_T(r) = -\partial\phi_T(r)/\partial r, \quad (3)$$

where

$$\frac{d\phi_T}{dr}(r) = H(r_{\text{break}} - r) \begin{cases} k_T^{(0)}(r - r_0) & \text{if } r < r_1, \\ k_T^{(1)}(r - \tilde{r}_1) & \text{if } r \geq r_1. \end{cases} \quad (4)$$

In equation (4), $H(r - r_{\text{break}})$ is the Heaviside function $H(a)$, which is defined to be zero for $a < 0$, and one for $a \geq 0$. The parameters $k_T^{(0)}$ and $k_T^{(1)}$ are the small and large-deformation spring constants. The parameter $\tilde{r}_1 = r_1 - k_T^{(0)}/k_T^{(1)}(r_1 - r_0)$ from force continuity conditions.

Intermolecular interactions between TC particles, HA particles and between HA and TC particles are described by a Lennard-Jones 12:6 (LJ) potential

$$\phi_{TC/HA/HA-TC}(r) = 4\varepsilon \left(\left[\frac{\sigma}{r} \right]^{12} - \left[\frac{\sigma}{r} \right]^6 \right), \quad (5)$$

with σ as the distance, and ε as energy parameter, defined separately for different materials.

Table 1. Summary of the parameters used in the mesoscopic molecular model, chosen based on atomistic modelling of solvated TC molecules, and model parameters for the HA crystal, as well as the HA–TC interactions ($1 \text{ kcal mol}^{-1} \text{ \AA}^{-1} = 69.479 \text{ pN}$).

Parameter and units	Value
Equilibrium bead distance, r_0 (in \AA)	7.00
Critical hyperelastic strain, r_1 (in \AA)	9.10
Bond breaking distance, r_{break} (in \AA)	10.5
Tensile stiffness parameter, $k_T^{(0)}$ (in $\text{kcal mol}^{-1} \text{ \AA}^{-2}$)	17.13
Tensile stiffness parameter, $k_T^{(1)}$ (in $\text{kcal mol}^{-1} \text{ \AA}^{-2}$)	195.32
Equilibrium angle, φ_0 (in deg)	180.00
Bending stiffness parameter, k_B (in $\text{kcal mol}^{-1} \text{ rad}^{-2}$)	15.00
Dispersive parameter TC–TC interactions, ε (in kcal mol^{-1})	2.8
Dispersive parameter TC–TC interactions, σ (in \AA)	15.984
HA crystal, ε (in kcal mol^{-1})	26.72
HA crystal, σ (in \AA)	3.118
Mass of each mesoscale particle (in amu)	500.00
Dispersive parameter HA–TC interactions, ε (in kcal mol^{-1})	25/15
Dispersive parameter HA–TC interactions, σ (in \AA)	7.00

The total energy is given by the sum over all pair-wise and three-body interactions ($I = \{T, \text{weak}, \text{HA}\}$):

$$E_I = \sum_{\text{pairs}} \phi_I(r) \quad \text{and} \quad E_B = \sum_{\text{angles}} \phi_B(\varphi). \quad (6)$$

2.3. Model parameters

Model parameters for TC properties and interactions are identical to those in [21]. The model parameters have been determined by hierarchical multi-scale modelling of more accurate, fully atomistic representations of solvated TC molecules and assemblies. This training set consists of a combination of first-principles ReaxFF reactive force fields and empirical CHARMM force fields [21]. In order to represent the interactions with the HA phase more accurately, a smaller bead-to-bead distance is chosen. The HA crystal is represented by a simple 2D triangular lattice described by a Lennard-Jones 12:6 (LJ) potential.

The parameter $\varepsilon_{\text{MF}} = 26.72 \text{ kcal mol}^{-1}$, with $\sigma_{\text{MF}} = 3.118 \text{ \AA}$, which leads to a Young’s modulus $E_{\text{HA}} \approx 135 \text{ GPa}$. These parameters are determined by fitting against the experimentally determined elastic modulus of HA [26, 27]. This 2D LJ model leads to extremely brittle material behaviour [28], thus providing a good model for the physical and mechanical properties of the HA phase.

Interactions between the HA crystal and TC molecules are described by a LJ potential with $\sigma_{\text{MF-TC}} = 7 \text{ \AA}$. The adhesion strength in this potential is chosen to be $\varepsilon_{\text{MF-TC}} = 25 \text{ kcal mol}^{-1}$ for all HA–TC interactions, while the beginning and end of each TC molecule interacts with $\varepsilon_{\text{MF-TC}} = 15 \text{ kcal mol}^{-1}$. The distinction of interaction mimics weaker adhesion between HA and TC at the head of each TC molecule due to smaller contact area. The choice of these parameters corresponds to interface surface energies of $\gamma_{\text{MF-TC}} \approx 0.375 \text{ J m}^{-2}$ and $\gamma_{\text{MF-TC}} \approx 0.225 \text{ J m}^{-2}$.

The parameters of the mesoscopic model are summarized in table 1.

Classical MD is used to solve the equations of motion by performing a continuous energy minimization of the system as the loading is increased, with a time step of 55 fs. After

energy minimization and relaxation of the initial structure, loading is applied by displacing a thin layer of particles at the ends of the system with a strain rate 7.558×10^{-8} per integration step. Periodic boundary conditions are applied in the direction orthogonal to pulling mimicking an infinitely large fibril, subject to uniaxial tensile loading.

It is emphasized that this simple model of the molecular and physical behaviour of the nanocomposite is designed to deliberately avoid modelling the atomistic details of bonding within the HA crystal or across the HA–TC interface. However, it enables one to model the inhomogeneous stress and strain fields as well as the fracture behaviour. Thus, the model system enables fundamental insight into the nanomechanics of mineralized fibrils.

2.4. Calculation of stress, tissue and component strain, strength and toughness

The stress is calculated based on the virial theorem [29], assuming an out-of-plane thickness of 15 \AA . The tissue strain is calculated based on the overall dimension change of the mineralized or non-mineralized CF. The component strains are averaged over several TC molecules and HA platelets to obtain good statistics.

The term ‘tissue strain’ (ε_T) refers to the uniaxial tensile strain applied to the CF or MCF, defined as $\varepsilon_T = \Delta L_x / L_{x,0}$ ($L_{x,0}$ is the initial length of the CF or MCF, and ΔL_x is the displacement). The extension ratio or stretch λ is related to the strain via $\lambda_i = 1 + \varepsilon_i$.

Energy dissipation is measured by considering the area under the stress–strain curve. The onset of yield is characterized by deviation from a linear elastic stress–strain relationship, typically followed by a sharp drop in stress. The fracture strength is defined as the maximum stress in the stress–strain curve. Toughness is characterized by large energy dissipation and high fracture strength.

3. Computational results

Figure 3 plots the stress–strain response of a pure collagen fibril (CF) compared with that of an MCF, under tensile loading, for tensile strains up to 50%. The stress–strain response for CF and MCF are qualitatively and quantitatively different, indicating that precipitation of HA crystals during bone formation significantly alters the material response. The MCF features a larger strength and much increased energy dissipation under deformation. Plastic deformation starts at approximately 6.7% tensile strain for the mineralized fibril, whereas it occurs at approximately 5% tissue strain in the case of a pure CF. Further, the MCF shows significant softening at larger strains, with a characteristic sawtooth-shaped stress–strain curve due to repeated intermolecular slip. The mineralized fibril features a higher stiffness than the pure collagen fibril.

Figure 4 shows snapshots of the molecular geometry under increasing tensile load, clearly showing the deformation mechanism of intermolecular slip. Figure 4(a) shows snapshots of the deformation mechanisms of pure CF. Fibrillar yield is characterized by intermolecular slip (see the circles highlighting a local area of repeated molecular slip). Slip leads

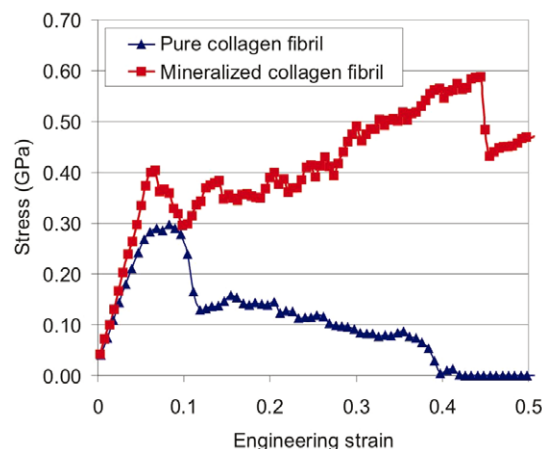


Figure 3. Stress–strain response of a mineralized collagen fibril (MCF) and a non-mineralized, pure collagen fibril (CF). The plot shows the stress–strain curve, for the entire deformation up to tensile tissue strains of 50%. It is apparent that the MCF features a larger strength and much increased energy dissipation under deformation. Plastic deformation starts at approximately 6.7% tensile strain for the mineralized fibril, whereas it occurs at approximately 5% tissue strain in the case of a pure CF. The MCF shows significant softening at larger strains, with a characteristic sawtooth-shaped stress–strain curve due to repeated intermolecular slip. The mineralized fibril is stiffer than the pure collagen fibril.

to formation of regions with lower material density. Figure 4(b) displays snapshots of the deformation mechanisms of MCFs. Slip initiates at the interface between HA particles and TC molecules. Slip reduces the density, leading to formation of nanoscale voids.

The details of the differences between the MCF and CF and associated deformation mechanisms will be discussed in the following sections.

3.1. Elastic and plastic deformation

Up to the onset of yield, the mechanical response of the MCF is elastic (within the range of normal physiological function). In this regime, the increase of tissue strain leads to continuous increase of the strain in each TC molecule. Both MCF and CF display a linear-elastic regime for small deformation. The MCF is 36% stiffer than the CF (the Young’s modulus of a CF is 4.59 GPa versus 6.23 GPa for an MCF). The presence of HA crystals further changes the onset of plastic deformation, characterized by a sudden drop in the stress–strain response. Whereas the CF begins to yield at approximately 5%, the MCF yields at 6.7%. This represents a 34% increase in yield strain. These results are summarized in table 2. The data shown in table 2 were generated based on the stress–strain curve shown in figure 3.

After the onset of yield, the stress does not drop to zero very quickly, but instead remains at a level of 0.4 GPa, with a slight increase with strain, approaching 0.6 GPa. After the onset of yield, the MCF becomes softer, that is, less force is required for identical extension. The reduction in slope is due to the fact the strain in some of the TC molecules does not increase with tissue strain, since an increasing number of bonds to HA crystals and other TC molecules are broken.

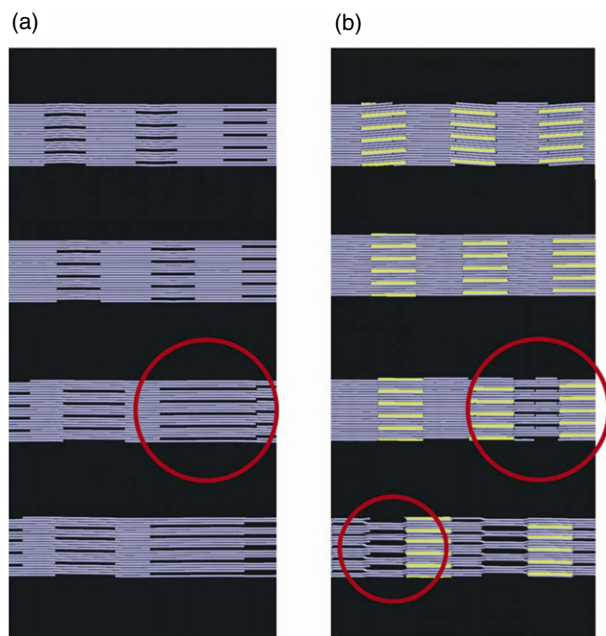


Figure 4. Molecular geometry of plastic deformation. Subplot (a): snapshots of the deformation mechanisms, pure CF, for increasing strain. Fibrillar yield is characterized by intermolecular slip (see the circles highlighting a local area of repeated molecular slip). Slip leads to formation of regions with lower material density. Subplot (b): snapshots of the deformation mechanisms, MCF, for increasing strain. Slip initiates at the interface between HA particles and TC molecules. Slip reduces the density, leading to formation of nanoscale voids.

When fracture occurs, all molecular bonds inside the MCF are broken, and the strains inside each component drop to zero.

Both CF and MCF yield by intermolecular slip. Repeated glide between TC molecules and between HA particles and TC molecules initiating by slip at the HA–TC interface enables a large regime of dissipative deformation after the beginning of yield. In the case of the MCF, larger stresses can be maintained after initiation of slip due to additional resistance to slip at the interface between the TC molecules and HA particles.

Mineralization of the CF leads to a factor of 2 increase in strength. Most importantly, mineralization leads to a five-fold increase in energy dissipation.

3.2. Molecular mechanisms of deformation and toughening

An analysis of the strain field within TC molecules and HA platelets reveals that the observations discussed in the previous section can be explained by molecular nanomechanical mechanisms, since mineralization significantly changes the strain distribution.

In pure CF, the tissue strain (applied strain) is always larger than the strain within TC molecules, reaching approximately 87% immediately before yield begins.

In MCF, the tissue strain and TC strain remain much closer during deformation, approaching similar strain levels at the onset of plastic deformation. This is due to the good adhesion between HA platelets and TC molecules, which hinders initiation of intermolecular slip. The HA phase carries

Table 2. Quantitative comparison of the deformation and fracture properties of CFs and MCFs (tensile strains up to 50%).

Property	CF	MCF	Ratio value MCF/CF
Young's modulus (small deformation)	4.59 GPa	6.23 GPa	1.36
Yield strain	5%	6.7%	1.34
Maximum stress	0.3 GPa	0.6 GPa	2
Failure mode	Molecular slip	Molecular slip and slip along HA–TC interface	N/A
Energy dissipation	3.83 GJ m ⁻³	19.48 GJ m ⁻³	≈5
Ratio of TC strain versus tissue strain	Approaches 87% at yield	Approaches 100% at yield	1.15
Ratio of HA strain versus tissue strain	N/A	11%	N/A
Size of fracture process zone ξ_{cr}	≈150 μ m	≈200 μ m	1.33

up to 11% of the tissue strain. Such large tensile strains correspond to a stress of several GPa.

Evidence for the molecular failure mechanisms of intermolecular slip is also found in experiment, as for instance shown in [23].

3.3. Comparison with experimental results

The most direct comparison of our molecular simulation results can be done with a recent experimental study reported in [23]. We briefly summarize the main findings. By carrying out tensile tests of MCFs obtained from mineralized turkey leg tendon, it was shown that the stiffness increases continuously with increasing mineral content. It was shown that different mineralization stages correspond to stiffness values from 500 MPa (low mineral content) to 3 GPa (high mineral content). Further, the experiments revealed that the stress–strain behaviour shows a characteristic softening behaviour: an initial, rather stiff regime persists up to strains of approximately 3%, which is followed by a significant softening. The observed stress–strain response is reminiscent of a bilinear softening stress–strain behaviour.

The mechanical behaviour calculated based on the molecular model of MCF reported in this paper agrees with several observations made in experiment [23]. For example, the MCF yield strain is in somewhat close to experimental results (3% in experiment and 6.7% in simulation) [23]. Further, the reduced slope at large strains agrees qualitatively with experiment [23].

The finding that Young's modulus increases is in qualitative accordance with experiment [23] comparing mineralized and non-mineralized tendon CFs. Experimental results suggest a continuous increase in Young's modulus under mineralization, ranging up to a factor of 3 for high mineral content [23].

Further, the finding that component strains are smaller than tissue strains are consistent with experiment in

bone [7, 27] and tendon [30], albeit these studies were carried out at larger scales. The results prove that this is also true at the smallest hierarchical scale of bone.

3.4. Local yield protects the integrity of the entire structure

The fracture process zone describes the geometric extension of the region around a crack-like flaw that undergoes plastic deformation when the specimen is loaded. For brittle materials, the fracture process zone is extremely small, limited to a few atomic distances. In ductile materials, the fracture process zone can become very large, approaching the specimen dimensions.

The size of the plastic, dissipative zone for a crack oriented orthogonal to the alignment direction of TC molecules can be approximated as

$$\xi_{\text{cr}} \approx \frac{2\gamma E}{\sigma_{\text{max}}^2}, \quad (7)$$

where σ_{max} is the maximum fracture stress, γ is the energy necessary to create a new surface, and E is Young's modulus. Equation (7) shows that the size of the fracture process zone is proportional to the fracture surface energy. Thus increases in the dissipative work required to create two new surfaces lead to much larger plastic zones.

Based on the parameters for extracted from molecular simulation (numerical values for E and σ_{max} are given in table 2; $\gamma = 11\,460 \text{ J m}^{-2}$) $\xi_{\text{cr}} \approx 400 \text{ }\mu\text{m}$ for MCFs.

This length scale has another important implication: for any defect smaller than ξ_{cr} , fracture will not be controlled by the presence of this flaw. The material is insensitive to the presence of crack-like flaws below this characteristic defect dimension.

Notably, this length scale is of the same order of magnitude as small microcracks typically found in bone, with characteristic dimensions of several hundred micrometres in diameter [6]. It may also play a significant role in bone remodelling. Bone is remodelled in so-called basic multicellular units (BMUs), a combination of osteoclasts and osteoblasts forming small cavities inside the tissue. It has been shown that BMUs represent defects with dimensions of approximately $200 \text{ }\mu\text{m}$, thus of similar orders of magnitude as ξ_{cr} [6, 31]. Thus the particular properties of MCF could be a vital component in allowing the presence of BMUs inside the tissue without compromising its strength.

Further, by limiting the dimensions of individual MCFs in the hierarchical structure, failure will occur homogeneously within each MCF, with plastic strains distributed over the entire geometry [19, 32].

This analysis provides insight into how the particular MCF structure contributes to toughness by comparing a pure HA crystal. The surface energy of pure HA ranges from 0.3 to 1.6 J m^{-2} (density functional theory calculations [33]), leading to a rather small fracture process zone of the order of several nanometres. Thus any larger crack-like defect larger will lead to catastrophic failure. The estimate for γ of an MCF obtained from MD studies of a fibril is several orders of magnitudes higher. Even though the modulus is much reduced in comparing a pure HA crystal with the MCF, the significant increase in γ outruns the reduction in modulus. Further, the fact that σ_{max} is smaller further leads to increase in the length scale.

In comparison with a CF, the MCF has a larger fracture process zone due to an increase in γ as well as an increase in E . The effect of these two parameters exceeds the effect of a smaller σ_{max} .

4. Discussion

The work overcomes the limitations of the existing models of bone by explicitly considering TC molecules interacting with HA phases, providing a physics-based material description that enables one to make direct links between molecular structure, topology and fracture behaviour. It is found that the nanostructural arrangement of the MCF is key to its mechanical properties, notably by allowing molecular slip as a major toughening mechanism.

In the following sections, implications of the findings for the understanding of bone formation and bone mechanics are discussed.

4.1. Hierarchical toughening mechanisms

Past research has revealed that toughening occurs at different scales [8, 10, 13]. Our studies and results from investigations at other length scales suggest that each level in the hierarchy of bone may be designed to provide optimal toughness, thus being capable of taking advantage of nanoscale molecular and crystal properties, at larger scales.

The behaviour discussed in this paper is qualitatively similar to that suggested by the sacrificial bond model [11]. However, the mechanism described here operates at a smaller length scale in bone's structural hierarchy, and has a different nanostructural origin; it is closely linked to the particular staggered molecular structure of the collagen fibrils and does not involve the presence of metal ions. It is found that at the level of individual MCFs, intermolecular slip is a major mechanism of dissipation (see, for instance, in figure 4).

To enable this dissipation mechanism, the adhesion energy between HA crystals and TC molecules must be in a critical regime. This regime is characterized by the following condition: it must allow strengthening by making it more difficult to initiate molecular slip, but it must be small enough so that covalent bonds inside the tropocollagen molecules are not broken. Interface energies of the order of magnitude that allow for these deformation mechanisms correspond to ionic interactions across the TC-HA interface. Indeed, ionic interactions have recently been suggested based on NMR studies of a TC-HA interface in physiological bone [34, 35].

Pure van der Waals (vdW) or H-bond interactions would lead to adhesion energies of approximately 0.01 J m^{-2} . This would be insufficient to make MCFs stronger or increase the toughness, thus rendering the presence of minerals in the gap regions insignificant. In the other extreme case, increasing $\gamma_{\text{MF-TC}}$ to values corresponding to covalent bonds ($\gamma_{\text{MF-TC}} > 1 \text{ J m}^{-2}$), the deformation mechanics changes so that plastic yield does not set in until TC molecule rupture occurs, leading to a shutdown of the toughening mechanism.

The large aspect ratio of the mineral platelets leads to large shear forces between the TC molecule and the HA crystal, since $F_{\text{shear}} \sim A_c$ ($A_c \sim L_c$ is the contact area between TC and HA).

The analysis of the strain distribution inside the MCF shows that the stress in HA platelets approaches several GPa. However, macroscopic HA crystals that break at 0.1% tensile strain and stresses as low as 65 MPa [7]. It was shown in earlier studies that by reducing the size of an HA crystal to dimensions below 30 nm, the strength of the crystal approaches the theoretical value, even under presence of cracks or other defects [13, 19]. Under flaw-tolerant conditions, the material does not sense the existence of defects and is thus capable of reaching its theoretical strength. Thus the flaw-tolerance concept could be a possible explanation for the fact that mineral platelets can sustain large stresses that approach 1 GPa, without fracturing.

4.2. Molecular design scenarios

Our model enables one to develop different design scenarios. As reported in a previous study [36], high cross-link densities in a pure CF without HA phase make the material stronger, but lead to a brittle polymer with low toughness and low stiffness. Such behaviour is undesirable for the physiological role of bone.

As shown in the analyses reported in this paper, adding very stiff ceramic platelets inside the collagen fibril represents a strategy to insert high densities of covalent chemistry in order to make the material stiffer and stronger without compromising toughness. The addition of mineral platelets allows the material to yield under large load in order to protect the entire structure. The molecular role of HA platelets in MCFs thus appears to be related to the increase of the strength by providing a larger energy barrier against intermolecular slip. At the same time, the presence of HA platelets increases the dissipative nature of large-strain deformation of MCFs. Also, the molecular arrangement of MCFs allows one to achieve a good weight–strength efficiency, since the dominating protein phase is lighter than the HA phase.

As discussed in a previous study [21], the length of TC molecules controls the mechanical behaviour of CFs, and we expect a similar behaviour for MCFs. Short TC molecules lead to reduced strength and MCFs may become rather brittle. Long tropocollagen molecules are vital to yield large toughness, as they provide a means to enable long deformation paths with large slipping inside the material. The physiological significance of toughness may explain why extremely long TC molecules in MCFs are a highly conserved molecular feature [1, 3, 5, 8, 37]. However, if the TC molecules become too long, utilization of the intermolecular ‘glue’ becomes inefficient [21]. As shown in an earlier study [21], molecular lengths at approximately 200 nm provide the most optimal basis for CFs. Further analysis of the dependence of mechanical properties of MCFs on the TC molecule length is left to future studies.

The molecular toughening mechanism described in this work unifies controversial attempts of explaining sources of toughness of bone, as it illustrates that both crack tip mechanisms [14, 15] and flaw tolerance concepts [19] play a key role in the mechanical response of bone under extreme load.

In addition to mineralizing CFs, structural features at larger length scales of bone, the dependence of material

properties on time (e.g. via osteoblast and osteoclast cells [3]), and extrafibrillar matrix properties [10] are important for the macroscopic mechanical properties of bone. However, our results clearly show the significance of the nanoscale TC–HA patterning as a toughening mechanism at the nanoscale and microscale.

4.3. Bone formation and tissue growth

Our analysis shows that the particular properties of MCF allow it to tolerate cracks with dimensions of several hundred micrometres; this may be critical to enable the operation of basic molecular units (BMUs), which require the presence of small cavities inside the tissue, in the repair of bone [6].

The mechanical properties of a scaffolding material can influence the growth rate and quality of the bone tissue [38], providing evidence that not only chemical growth factors, but also the nano- and micromechanical material properties, play a role in tissue development.

Further, it has been shown that the presence of a stiff matrix directs stem cell differentiation towards osteoblasts [39]. Thus the increase in stiffness due to mineralization—as shown in figure 3 and table 2—could be a critical aspect during the formation of nascent bone.

5. Conclusion

The studies reveal that the mechanical properties of CF change significantly after mineralization. Whereas pure TC fibrils are soft and the HA minerals are stiff and extremely fragile, the stiffness of mineralized fibrils assumes intermediate values, but with much increased energy dissipation during deformation. Table 2 summarizes the main effects of mineralization. Important structural features in MCFs and their effects on the mechanical behaviour are:

- The presence of HA crystals, to provide additional resistance against plastic deformation, to increase Young’s modulus and the fracture strength.
- Adhesion forces between HA and TC remain weak enough, to allow for slip under large load instead of inducing fracture inside the TC molecules, but strong enough to provide significant strengthening.
- Characteristic nanoscopic dimensions, to utilize the intermolecular adhesion forces most efficiently.
- Further, as illustrated in a previous study [21], the presence of long TC molecules in order to provide the basis for long deformation paths for high energy dissipation.

Modifications of the mechanical properties of CF under mineralization control the fracture properties of MCFs. Our analysis reveals that the particular constitutive behaviour of MCFs induces a crack tip mechanism known as plastic shielding, effectively increasing the toughness of the tissue. The concept behind this mechanism is to sacrifice a small part of the structure in order to rescue the integrity of the entire structure. The presence of large yield regions of the order of several hundred micrometres leads to a more equal stress distribution under loading and enables the operation of BMUs. In contrast, cracks in pure HA crystals lead to

potentially dangerous large stress concentrations around flaws. The concept of equal stress distribution is known as a driving force for topology and shape evolution of natural structures such as bone and trees. The results suggest that this appears to be a universal principle that also holds at the nanoscale.

Development of the yield region represents a toughening mechanism whose origin is intimately linked with molecular geometry and mechanisms, underlining the significance of nanostructure for bone properties. The results provide molecular-scale explanations of experiments that show an increase in yield stress [40] and maximum fracture stress [41], as well as failure strength [42] with increasing mineral content.

An important trait of protein materials is that they display highly specific hierarchical structures, from nanoscale to macroscale. Some of these features are commonly found in different species and tissues; that is, they are highly conserved. Examples include alpha-helices, beta-sheets or collagen fibrils that represent universal building blocks forming the basis for diverse range of protein materials. In contrast, other features are highly specific to species or tissue types, such as tendon fascicles or beta-sheet nanocrystals in spider silk. Universal features in protein materials are most common at the nanoscale, as can be seen in examples such as the beta-strand motif, alpha-helices or collagen fibrils. Structural diversity becomes more prominent at larger scales. Biological materials often feature a coexistence of universality and diversity. Universality is linked to robustness; diversity is linked to optimality. The collagen fibril motif—one of the most abundant protein structures found in biology—may be highly conserved since it provides a very robust means to achieve highly dissipative materials. Notably, instead of creating a multitude of distinct secondary protein structures, nature creates complexity through hierarchies and internal degrees of freedom that arise from the lower scale. Through applying hierarchies, nature keeps the opportunity to adapt systems without significantly changing their structure. The formation of hierarchical structures enables one to overcome the physical limitations of a scale-specific design space. By simultaneously adapting a multitude of structures at different length scales, it is possible to create materials whose properties by far exceed those of each constituent or those that could be reached at a single scale alone. Understanding the fundamentals of this trait of biological materials could lay the foundation for a new class of biomimetic materials in which precisely controlled hierarchical features are exploited to tailor their properties.

Acknowledgment

MJB acknowledges support from the National Science Foundation (NSF CAREER Award, program manager Dr Jimmy Hsia).

References

- [1] Currey J D 2002 *Bones: Structure and Mechanics* (Princeton, NJ: Princeton University Press)
- [2] Currey J D 2005 Materials science—hierarchies in biomineral structures *Science* **309** 253–4
- [3] Weiner S and Wagner H D 1998 The material bone: structure mechanical function relations *Annu. Rev. Mater. Sci.* **28** 271–98
- [4] Jager I and Fratzl P 2000 Mineralized collagen fibrils: a mechanical model with a staggered arrangement of mineral particles *Biophys. J.* **79** 1737–46
- [5] Fratzl P *et al* 2004 Structure and mechanical quality of the collagen–mineral nano-composite in bone *J. Mater. Chem.* **14** 2115–23
- [6] Taylor D, Hazenberg J G and Lee T C 2007 Living with cracks: damage and repair in human bone *Nat. Mater.* **6** 263–6
- [7] Gupta H S *et al* 2006 Cooperative deformation of mineral and collagen in bone at the nanoscale *Proc. Natl Acad. Sci. USA* **103** 17741–6
- [8] Gupta H S *et al* 2005 Nanoscale deformation mechanisms in bone *Nano Lett.* **5** 2108–11
- [9] Aizenberg J *et al* 2005 Skeleton of *Euplectella* sp.: structural hierarchy from the nanoscale to the macroscale *Science* **309** 275–8
- [10] Fantner G E *et al* 2005 Sacrificial bonds and hidden length dissipate energy as mineralized fibrils separate during bone fracture *Nat. Mater.* **4** 612–6
- [11] Thompson J B *et al* 2001 Bone indentation recovery time correlates with bond reforming time *Nature* **414** 773–6
- [12] Tai K, Ulm F J and Ortiz C 2006 Nanogranular origins of the strength of bone *Nano Lett.* **6** 2520–5
- [13] Gao H J 2006 Application of fracture mechanics concepts to hierarchical biomechanics of bone and bone-like materials *Int. J. Fract.* **138** 101–37
- [14] Nalla R K, Kinney J H and Ritchie R O 2003 Mechanistic fracture criteria for the failure of human cortical bone *Nat. Mater.* **2** 164–8
- [15] Nalla R K *et al* 2005 Fracture in human cortical bone: local fracture criteria and toughening mechanisms *J. Biomech.* **38** 1517–25
- [16] Ritchie R O *et al* 2004 Characteristic dimensions and the micro-mechanisms of fracture and fatigue in ‘nano’ and ‘bio’ materials *Int. J. Fract.* **128** 1–15
- [17] Ritchie R O *et al* 2006 Fracture and ageing in bone: toughness and structural characterization *Strain* **42** 225–32
- [18] Hansma P K, Turner P J and Ruoff R S 2007 Optimized adhesives for strong, lightweight, damage-resistant, nanocomposite materials: new insights from natural materials *Nanotechnology* **18** (4)
- [19] Gao H *et al* 2003 Materials become insensitive to flaws at nanoscale: lessons from nature *Proc. Natl Acad. Sci. USA* **100** 5597–600
- [20] Buehler M J 2006 Atomistic and continuum modeling of mechanical properties of collagen: elasticity, fracture and self-assembly *J. Mater. Res.* **21** 1947–61
- [21] Buehler M J 2006 Nature designs tough collagen: explaining the nanostructure of collagen fibrils *Proc. Natl Acad. Sci. USA* **103** 12285–90
- [22] Buehler M J and Wong S Y 2007 Entropic elasticity controls nanomechanics of single tropocollagen molecules *Biophys. J.* **93** 37–43
- [23] Gupta H S *et al* 2004 Synchrotron diffraction study of deformation mechanisms in mineralized tendon *Phys. Rev. Lett.* **93** (15)
- [24] Allen M P and Tildesley D J 1989 *Computer Simulation of Liquids* (Oxford: Oxford University Press)
- [25] Plimpton S 1995 Fast parallel algorithms for short-range molecular-dynamics *J. Comput. Phys.* **117** 1–19
- [26] Cuy J L *et al* 2002 Nanoindentation mapping of the mechanical properties of human molar tooth enamel *Arch. Oral Biol.* **47** 281–91
- [27] Borsato K S and Sasaki N 1997 Measurement of partition of stress between mineral and collagen phases in bone using x-ray diffraction techniques *J. Biomech.* **30** 955–7
- [28] Buehler M J, Abraham F F and Gao H 2004 Stress and energy flow field near a rapidly propagating mode I crack *Springer Lecture Notes in Computational Science and Engineering* (Berlin: Springer) pp 143–56
- [29] Tsai D H 1979 Virial theorem and stress calculation in molecular-dynamics *J. Chem. Phys.* **70** 1375–82

- [30] Screen H R C *et al* 2004 Local strain measurement within tendon *Strain* **40** 157–63
- [31] Turner C H 2006 Bone strength: current concepts *Skeletal Development and Remodeling in Health, Disease, and Aging (Annals of the New York Academy of Sciences)* vol 1068 (New York: New York Academy of Sciences) pp 429–46
- [32] Buehler M J *et al* 2006 Cracking and adhesion at small scales: atomistic and continuum studies of flaw tolerant nanostructures *Modelling Simul. Mater. Sci. Eng.* **14** 799–816
- [33] Zhu W H and Wu P 2004 Surface energetics of hydroxyapatite: a DFT study *Chem. Phys. Lett.* **396** 38–42
- [34] Wilson E E *et al* 2006 Three structural roles for water in bone observed by solid-state NMR *Biophys. J.* **90** 3722–31
- [35] Jaeger C *et al* 2005 Investigation of the nature of the protein–mineral interface in bone by solid-state NMR *Chem. Mater.* **17** 3059–61
- [36] Buehler M J 2007 Nanomechanics of collagen fibrils under varying cross-link densities: atomistic and continuum studies *J. Mech. Behavior Biomed. Mater.* at press
- [37] Cressey B A and Cressey G 2003 A model for the composite nanostructure of bone suggested by high-resolution transmission electron microscopy *Mineral. Mag.* **67** 1171–82
- [38] Alsberg E *et al* 2003 Regulating bone formation via controlled scaffold degradation *J. Dent. Res.* **82** 903–8
- [39] Engler A J *et al* 2006 Matrix elasticity directs stem cell lineage specification *Cell* **126** 677–89
- [40] Wachter N J *et al* 2002 Correlation of bone mineral density with strength and microstructural parameters of cortical bone *in vitro Bone* **31** 90–5
- [41] Louis O *et al* 1995 Cortical mineral-content of the radius assessed by peripheral QCT predicts compressive strength on biomechanical testing *Bone* **16** 375–9
- [42] Lotz J C, Gerhart T N and Hayes W C 1990 Mechanical-properties of trabecular bone from the proximal femur—a quantitative CT study *J. Comput. Assist. Tomogr.* **14** 107–14